Title

Dephosphorylation by protein phosphatase 2A regulates visual pigment regeneration and the dark adaptation of mammalian photoreceptors.

Journal

Proceedings of the National Academy of Sciences of USA, 114(45)

Authors

Kolesnikov, Alexander

Orban, Tivadar

Jin, Hui

et al.

Publication Date

2017-11-07

DOI

10.1073/pnas.1712405114

Peer reviewed

Dephosphorylation by protein phosphatase 2A regulates visual pigment regeneration and the dark adaptation of mammalian photoreceptors

Alexander V. Kolesnikov[a], Tivadar Orban[b], Hui Jin[b], Celine Brooks[c], Lukas Hofmann[b], Zhiqian Dong[d], Maxim Sokolov[c], Krzysztof Palczewski[b,1], and Vladimir J. Kefalov[a,1]

[a]Department of Ophthalmology and Visual Sciences, Washington University School of Medicine, St. Louis, MO 63110; [b]Department of Pharmacology, Case Western Reserve University, Cleveland, OH 44106; [c]Department of Ophthalmology, West Virginia University, Morgantown, WV 26506; and [d]Department of Medical Devices, Polgenix, Inc., Cleveland, OH 44106

Edited by Theodore G. Wensel, Baylor College of Medicine, Houston, TX, and accepted by Editorial Board Member Jeremy Nathans September 29, 2017 (received for review July 12, 2017)

Resetting of G-protein–coupled receptors (GPCRs) from their active state back to their biologically inert ground state is an integral part of GPCR signaling. This "on–off" GPCR cycle is regulated by reversible phosphorylation. Retinal rod and cone photoreceptors arguably represent the best-understood example of such GPCR signaling. Their visual pigments (opsins) are activated by light, transduce the signal, and are then inactivated by a GPCR kinase and arrestin. Although pigment inactivation by phosphorylation is well understood, the enzyme(s) responsible for pigment dephosphorylation and the functional significance of this reaction remain unknown. Here, we show that protein phosphatase 2A (PP2A) acts as opsin phosphatase in both rods and cones. Elimination of PP2A substantially slows pigment dephosphorylation, visual chromophore recycling, and ultimately photoreceptor dark adaptation. These findings demonstrate that visual pigment dephosphorylation regulates the dark adaptation of photoreceptors and provide insights into the role of this reaction in GPCR signaling.

PP2A | photoreceptors | GPCRs | visual cycle | dark adaptation

G-protein signaling is ubiquitous in living organisms where G-protein–coupled receptors (GPCRs) mediate responses to a variety of extracellular stimuli, from hormonal activity and cell-to-cell communication to sensory transduction (1). The activity of GPCRs is regulated by their phosphorylation by cellular kinases and dephosphorylation by phosphatases. Typically, the unphosphorylated (active) form of the receptor initiates a cascade of signaling events, and its subsequent phosphorylation by a relevant G-protein–coupled receptor kinase (GRK), followed by arrestin binding, converts it to an inactive state, thereby terminating the signaling (2, 3).

Phototransduction in rod and cone photoreceptor neurons of the retina is one of the best-characterized G-protein–signaling cascades (4–6). It starts with the activation of a visual pigment by a photon of light. This prototypical GPCR consists of an apoprotein (rod or cone opsin) covalently bound to a visual chromophore, 11-*cis*-retinal (7). Absorption of a photon by the chromophore induces its isomerization from the ground 11-*cis*- state to an all-*trans*- conformation (8). This activates the visual pigment, which in turn activates multiple copies of the G-protein transducin, triggering the phototransduction cascade that leads to closure of outer segment cGMP-gated channels and hyperpolarization of the photoreceptor (9). Similar to other G-protein cascades, visual pigment inactivation in photoreceptors is initiated by phosphorylation by cell-specific GRKs that partially inactivates the pigment (10, 11). Subsequent binding of arrestin fully inactivates the pigment, leading to the eventual termination of the light response (12, 13).

Despite tremendous progress in this field, the enzyme that carries out the subsequent dephosphorylation of the pigment and the role of this reaction in photoreceptor function and survival remain unknown. In *Drosophila*, this role is served by the retinal degeneration C (rdgC) phosphatase (14). *Drosophila* rdgC has a high degree of sequence homology to vertebrate protein phosphatases PPEF-1 and PPEF-2 (15). However, experiments with PPEF-1/PPEF-2 double-knockout mice have ruled out the involvement of these enzymes in vertebrate photoreceptors (16). Several other putative pigment phosphatases have been identified in vertebrate photoreceptors, including latent phosphatase 2 (17), protein kinase FA (17), calcium-activated opsin phosphatase (18), and protein phosphatase type 2C (19). Finally, based on enzymatic assays, the type 2A protein phosphatase (PP2A) also has been proposed to be the putative rhodopsin phosphatase (20–22). However, the rate of opsin dephosphorylation by PP2A observed in vitro was found to be lower than the rates for other PP2A substrates (23), raising doubt about the functional significance of this reaction. Other GPCRs, such as the β-adrenergic receptor, could also be dephosphorylated by PP2A (24, 25). Previous attempts at understanding the involvement of PP2A in the dephosphorylation of GPCRs have failed due to its embryonic lethality in mice with conventional knockout of its dominant catalytic subunit PP2A-Cα (26) or its major scaffolding subunit PP2A-Aα (27).

Here, we used a different approach to ablate PP2A-Cα selectively in mouse rod or cone photoreceptors. We then employed biochemical and physiological analyses to investigate the role of

Significance

Resetting G-protein–coupled receptors (GPCRs) from their active state to their biologically inert ground state driven by reversible phosphorylation and arrestin binding is an integral part of GPCR signaling. Visual pigments in retinal rod and cone photoreceptors represent a classic example of GPCR signaling. Although pigment inactivation by phosphorylation is well understood, the enzyme(s) responsible for pigment dephosphorylation and the functional significance of this reaction remain largely unknown. Here, we show that protein phosphatase 2A (PP2A) is expressed in mouse photoreceptors and that its targeted ablation compromises, but does not fully block, their pigment dephosphorylation, visual chromophore recycling, and dark adaptation after >90% bleach. We conclude that visual pigments are dephosphorylated by PP2A and that this reaction regulates dark adaptation of photoreceptors.

Author contributions: A.V.K., K.P., and V.J.K. designed research; A.V.K., T.O., H.J., C.B., L.H., Z.D., M.S., and V.J.K. performed research; A.V.K., T.O., H.J., L.H., Z.D., M.S., K.P., and V.J.K. analyzed data; and A.V.K., K.P., and V.J.K. wrote the paper.

The authors declare no conflict of interest.

This article is a PNAS Direct Submission. T.G.W. is a guest editor invited by the Editorial Board.

[1]To whom correspondence may be addressed. Email: kxp65@case.edu or kefalov@vision.wustl.edu.

This article contains supporting information online at www.pnas.org/lookup/suppl/doi:10.1073/pnas.1712405114/-/DCSupplemental.

this enzyme in both pigment dephosphorylation and in the function of photoreceptors. As PP2A has also been suggested to dephosphorylate another abundant rod phosphoprotein, phosducin, in a light-dependent manner (23, 28), we also examined the state of phosducin phosphorylation in rods lacking PP2A-Cα.

Results

Retinal Morphology in Rod-Specific PP2A-Cα Knockout Mice. Despite the fact that many protein phosphatases are present in mammalian retinal photoreceptors (29), the identity of the enzyme that dephosphorylates visual pigments following their activation by light in vivo remains uncertain. To investigate the role of the putative rhodopsin phosphatase PP2A in photoreceptors, we generated mice in which the major isoform of the catalytic subunit of PP2A (PP2A-Cα) was flanked by LoxP sites (*Ppp2ca*$^{f/f}$) (Fig. 1*A*). This allowed us to selectively target the expression of PP2A in rods by crossing PP2A-floxed mice with the rod-specific *Cre* mouse line *iCre75* (30) to generate rod-specific PP2A conditional knockout (*Ppp2ca*$^{f/f}$ *iCre75*$^{+}$) mice.

In situ mRNA hybridization using an RNAscope assay produces a characteristic semiquantitative punctate staining generated by signal amplification from single-transcript molecules (31). Such an analysis of retinal sections demonstrated an abundant expression of PP2A-Cα transcripts throughout the retinas of control mice, including in their photoreceptor inner segment layer (Fig. 1*B*, *Center*). This result, consistent with previous studies (20–22), demonstrated the robust expression of PP2A in mammalian photoreceptors. A similar analysis in *Ppp2ca*$^{f/f}$ *iCre75*$^{+}$ mice revealed that PP2A-Cα expression in the inner segment layer of their retinas was greatly reduced (Fig. 1*B*, *Right*). As rods represent the bulk of photoreceptors in mouse retina, this result clearly demonstrates that expression of PP2A was successfully eliminated from the rods of *Ppp2ca*$^{f/f}$ *iCre75*$^{+}$ mice. The residual signal in the inner segment layer of these mutant mice likely reflects the expression of PP2A-Cα in the sparse cone photoreceptors. In contrast, PP2A-Cα expression in the inner retina was unaffected in *Ppp2ca*$^{f/f}$ *iCre75*$^{+}$ mice, confirming the rod specificity of its ablation. Also consistent with the successful deletion of PP2A-Cα selectively in rods, qRT-PCR analysis demonstrated a significant reduction (34%, $P < 0.01$) in total PP2A-Cα mRNA in *Ppp2ca*$^{f/f}$ *iCre75*$^{+}$ retinas compared with *iCre75*$^{+}$ controls, with the remaining 66% expression derived from cones and the inner retina (Fig. 1*C*, *Left*). Importantly, the minor PP2A-Cβ subunit transcript level was not up-regulated in response to the deletion of PP2A-Cα from rods (Fig. 1*C*, *Right*).

We next investigated the expression of PP2A-Cα protein in photoreceptors by fluorescence immunohistochemistry, which produced a robust immunofluorescence signal within the photoreceptor layer of control mice (Fig. 1*D*, *Left*). Notably, most of the PP2A signal was located in the outer segment layer, an observation consistent with its proposed role of dephosphorylating the visual pigment. PP2A-Cα immunofluorescence was greatly reduced in the photoreceptor layer of *Ppp2ca*$^{f/f}$ *iCre75*$^{+}$ retinas

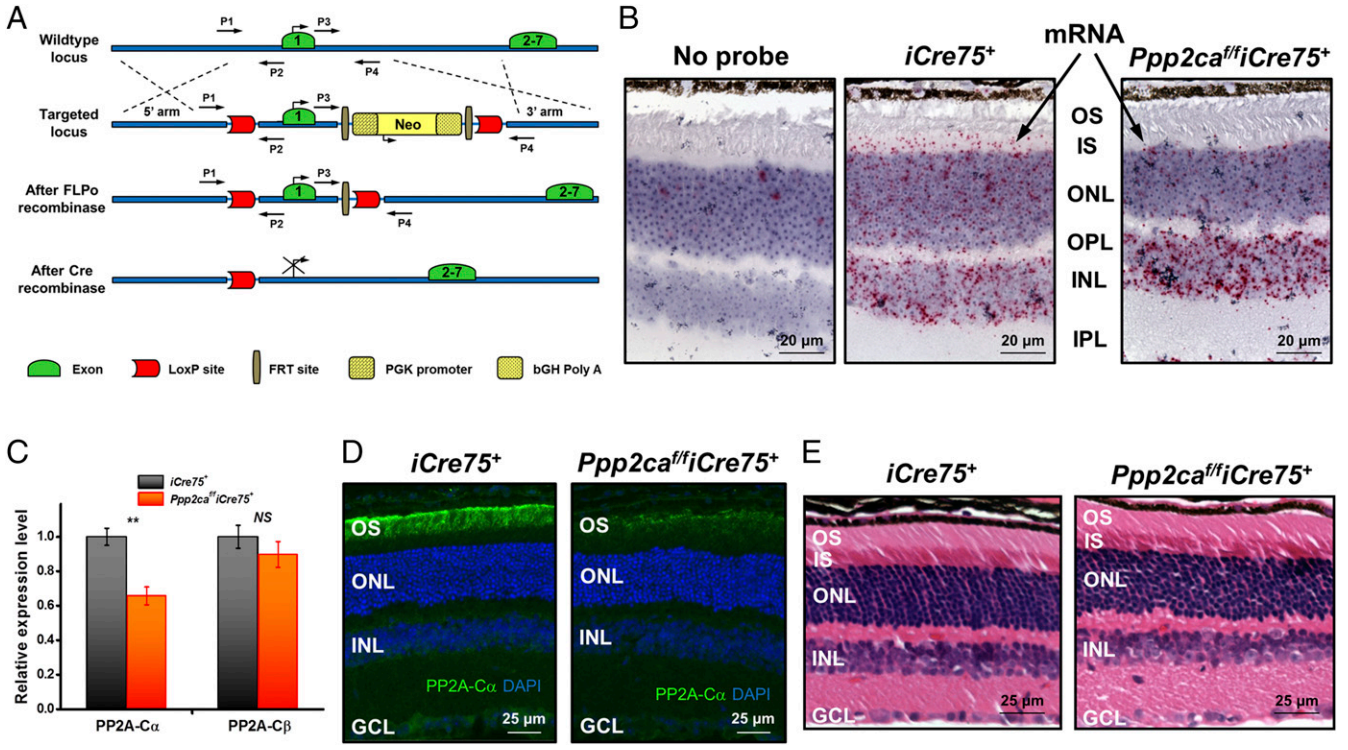

Fig. 1. Genetic and morphological characterization of rod photoreceptor-specific PP2A-Cα knockout mice. (*A*) Generation of the conditional PP2A-Cα knockout mouse. The vector for targeting *Ppp2ca* exon 1 contains a 5′ homology arm, a conditional arm with a single *LoxP* site upstream of it, a PGK promoter-driven removable *Frt-Neo-Frt* cassette with a *LoxP* site downstream of it, and a 3′ homology arm. Dashed crossover lines show the sites of homologous recombination used to produce the targeted *Ppp2ca* allele. The *Frt-Neo-Frt* cassette was excised by crossing with transgenic mice expressing *FLPo* recombinase. The bottom sketch shows the disrupted *Ppp2ca* gene after *Rho-Cre*–mediated recombination, with the arrow indicating the position of the ATG start codon in exon 1. P1–P4 are primers used for genotyping (*Materials and Methods*). (*B*) Absence of PP2A-Cα mRNA in rods of PP2A-Cα knockout mice. In situ hybridization of 4-mo-old *iCre75*$^{+}$ control (*Center*) and *Ppp2ca*$^{f/f}$ *iCre75*$^{+}$ (*Right*) mouse retinas with the PP2A-Cα probe (RNAscope, ACD). *Left* shows no signal in the control retina in the absence of the probe. INL, inner nuclear layer; IPL, inner plexiform layer; IS, inner segments; ONL, outer nuclear layer; OPL, outer plexiform layer; OS, outer segments. (Scale bar, 20 μm.) (*C*) Relative expression of PP2A-Cα mRNA in whole retinas of *iCre75*$^{+}$ control ($n = 5$) and *Ppp2ca*$^{f/f}$ *iCre75*$^{+}$ ($n = 5$) mice examined by qRT-PCR. Error bars represent SEM. Student's *t* test, $^{**}P < 0.01$; NS (not significant): $P > 0.05$. (*D*) Immunostaining of *iCre75*$^{+}$ control and *Ppp2ca*$^{f/f}$ *iCre75*$^{+}$ retinas with anti-PP2A-Cα antibody (green). Cell nuclei were stained with DAPI (blue). (Scale bar, 25 μm.) (*E*) Comparison of retina and photoreceptor morphology in H&E-stained sections of retinas from 5-mo-old *iCre75*$^{+}$ control and *Ppp2ca*$^{f/f}$ *iCre75*$^{+}$ mice. GCL, ganglion cell layer; INL, inner nuclear layer; IPL, inner plexiform layer; IS, inner segments; ONL, outer nuclear layer; OPL, outer plexiform layer; OS, outer segments. (Scale bar, 25 μm.)

(Fig. 1*D*, *Right*), demonstrating the ablation of PP2A from rods. Similar to our in situ mRNA hybridization results, residual PP2A-Cα immunofluorescence was observed in some outer segments that most likely reflected the expression of PP2A in cones.

Finally, we investigated whether the rod-specific deletion of PP2A-Cα affects retinal morphology. Examination of retinal sections revealed normal outer retina morphology in PP2A-deficient mice. Even in 5-mo-old animals, the thickness of the outer nuclear layer, the inner segment layer, and the outer segment layer was comparable in control and *Ppp2ca*$^{f/f}$ *iCre75*$^{+}$ retinas (Fig. 1*E*). Thus, perhaps surprising considering the ubiquitous expression of this enzyme, the deletion of PP2A-Cα in rods did not cause detectable retinal degeneration. The lack of morphological changes or photoreceptor cell loss in *Ppp2ca*$^{f/f}$ *iCre75*$^{+}$ mice allowed a rigorous physiological and biochemical characterization of these animals to determine the role of PP2A in rod pigment and phosducin dephosphorylation as well as in rod function.

Phototransduction in PP2A-Cα–Deficient Rods. To determine whether the deletion of PP2A-Cα affects the phototransduction cascade of mouse rods and their physiological function, we first performed single-cell recordings from dark-adapted rods with a suction electrode (Fig. 2). If PP2A were the only enzyme dephosphorylating mouse rhodopsin, a significant fraction of the pigment would be expected to remain phosphorylated in PP2A-deficient rods, even after overnight dark adaptation. As rhodopsin phosphorylation reduces its efficiency of activating the phototransduction cascade (32), this would be expected to reduce the amplification of phototransduction and lower the photosensitivity of dark-adapted rods. These recordings also allowed an evaluation of the overall health of PP2A-deficient rods and their signaling.

In agreement with the similar lengths of their outer segments, dark-adapted *Cre* control and PP2A-deficient rods produced saturated responses of comparable amplitudes (Fig. 2 *A* and *B* and Table 1). Notably, the photosensitivity of *Ppp2ca*$^{f/f}$ *iCre75*$^{+}$ rods was also normal after overnight dark adaptation (Fig. 2*C* and Table 1). The dim flash responses of rods lacking PP2A-Cα were comparable to those of control *iCre75*$^{+}$ rods, with only a slight but statistically significant increase in the time to peak (Fig. 2*D* and Table 1). The reason for the slightly broader peak of dim flash responses in PP2A-deficient rods is unclear, and considering the ubiquitous regulatory nature of PP2A, it could be caused by slight changes in any of a number of phototransduction steps. As rhodopsin inactivation occurs significantly faster than the rate-limiting inactivation of rod transducin (50 vs. 200 ms; e.g., ref. 33), it is unlikely that the slight change in response kinetics reflects changes in rhodopsin inactivation kinetics. Importantly, both phototransduction activation, measured from the rising phase of the dim flash response, and its late inactivation, characterized by the response recovery time constant τ_{rec}, were unaffected by the deletion of PP2A-Cα (Fig. 2*D* and Table 1). Finally, the response recovery following saturating flashes was also normal in PP2A-deficient rods, as indicated by the comparable dominant recovery time constants (τ_D) determined from a series of supersaturating flashes (Fig. 2*D*, *Inset*). Interestingly, our experimental τ_D values for both control *iCre75*$^{+}$ and mutant *Ppp2ca*$^{f/f}$ *iCre75*$^{+}$ rods (89 and 95 ms, respectively) were substantially lower than those (~200 ms) typically reported for mouse rods (34). However, this difference can be attributed to the acceleration of phototransduction shutoff in *iCre75*$^{+}$ mouse rods (35). Despite this complication, the use of proper *Cre* controls for our physiological recordings allowed a reliable evaluation of the effect of PP2A-Cα ablation on rod function. Taken together, these results indicate that elimination of the major catalytic subunit of PP2A in mouse rods does not compromise their phototransduction and signaling under dark-adapted conditions. The normal dark current and sensitivity in PP2A-deficient rods are consistent with the morphological data above and demonstrate that the deletion of PP2A-Cα does not affect rod overall health or survival. Finally, the normal dark-adapted sensitivity of PP2A-deficient rods indicates that, after overnight dark adaptation, their visual pigment is dephosphorylated despite the absence of PP2A.

Suppressed Rod Dark Adaptation in Mice with Rod-Specific Ablation of PP2A-Cα. The results above clearly demonstrate that deletion of PP2A-Cα does not affect the function of rods under dark-adapted conditions. To investigate whether dephosphorylation of visual pigment by PP2A is required for the timely dark adaptation of mouse rods, we next determined the kinetics of rod dark adaptation in vivo by electroretinography (ERG). Rod dark adaptation was measured by tracking the recovery of rod ERG a-wave amplitude and sensitivity after nearly complete (>90%) bleaching of the rod visual pigment. Under these in vivo conditions, dark adaptation of rods is driven by the efficient decay of

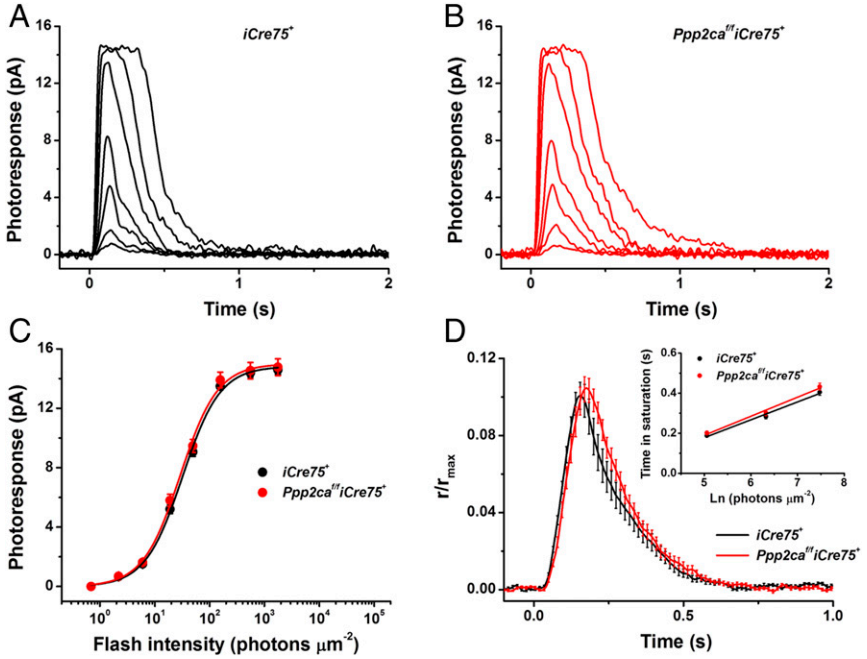

Fig. 2. Light responses of control and PP2A-Cα–deficient mouse rods. (*A*) Representative family of flash responses from a *iCre75*$^{+}$ control mouse rod. Test flashes of 500-nm light with intensities of 2.2, 6.0, 19.0, 49.5, 157, 557, and 1,764 photons·μm^{-2} were delivered at time 0. (*B*) Representative family of flash responses from a *Ppp2ca*$^{f/f}$ *iCre75*$^{+}$ mouse rod. Test flashes of 500-nm light had the same intensities as in *A*. (*C*) Averaged rod intensity–response functions (mean ± SEM) for *iCre75*$^{+}$ control (n = 16) and *Ppp2ca*$^{f/f}$ *iCre75*$^{+}$ (n = 15) mice. Hyperbolic Naka–Rushton fits yielded half-saturating intensities ($I_{1/2}$) of 32 and 29 photons·μm^{-2} for control and PP2A-Cα–deficient rods, respectively. (*D*) Kinetics of phototransduction activation and inactivation in *iCre75*$^{+}$ control (n = 16) and *Ppp2ca*$^{f/f}$ *iCre75*$^{+}$ (n = 15) rods. Population-averaged (mean ± SEM) dim-flash responses to light intensity of 6.0 photons·μm^{-2} were normalized to their respective maximum dark currents (R_{max}). The *Inset* shows determination of the dominant recovery time constant (τ_D; mean ± SEM) from a series of supersaturating flashes. Linear fits of the data yielded τ_D values of 89 and 95 ms for control and PP2A-deficient rods, respectively.

Table 1. Parameters of single-cell responses from dark-adapted mouse rods

Response parameter	Control rods (n = 16)	PP2A-deficient rods (n = 15)
I_{dark}, pA	14.6 ± 0.3	14.8 ± 0.6 NS
T_{peak}, ms	155 ± 4	178 ± 5***
$T_{integr.}$, ms	202 ± 11	216 ± 9 NS
S_f, $\mu m^2 \cdot photon^{-1}$	$1.8 \times 10^{-2} \pm 1.0 \times 10^{-3}$	$1.8 \times 10^{-2} \pm 1.0 \times 10^{-3}$ NS
$I_{1/2}$, $photon \cdot \mu m^{-2}$	32 ± 2	29 ± 2 NS
$n(I_{1/2})$	1.35 ± 0.02	1.34 ± 0.03 NS
τ_{rec}, ms	135 ± 10	140 ± 9 NS

I_{dark}, dark current measured from saturated responses; time to peak (T_{peak}), integration time ($T_{integr.}$), and normalized flash sensitivity (S_f) refer to responses whose amplitudes were ~0.2 I_{dark} and fell within the linear range; $I_{1/2}$, half-saturating light intensity; $n(I_{1/2})$, Hill coefficient in the Naka–Rushton equation; τ_{rec}, time constant of single-exponential decay of the dim flash response recovery phase. Data are given as mean ± SEM. Student's t test, NS indicates $P > 0.05$; ***$P < 0.001$ compared with control values.

photoactivated visual pigment and its subsequent regeneration with fresh 11-*cis*-chromophore supplied by the retinal pigment epithelium (RPE).

First, we recorded rod-driven scotopic ERG responses in the dark and found that they were of similar waveforms and maximal amplitudes in control *iCre75*$^{+}$ (296 ± 12 μV, n = 14) and mutant *Ppp2ca*$^{f/f}$ *iCre75*$^{+}$ mice (328 ± 14 μV, n = 14, $P > 0.05$) (Fig. 3*A*). This finding once again indicates that the total number of rods is preserved and their signaling is not suppressed by the deletion of PP2A-Cα. Furthermore, *Ppp2ca*$^{f/f}$ *iCre75*$^{+}$ mice produced normal ERG b-waves, suggesting that rod signal transmission to ON-bipolar cells is also normal in retinas with PP2A-deficient rods. Next, mice were exposed to brief bright light to bleach the bulk of their pigment, and then the recovery of their responses was monitored during the following dark-adaptation period. Immediately after a nearly complete pigment bleach, rods in both control *iCre75*$^{+}$ and mutant *Ppp2ca*$^{f/f}$ *iCre75*$^{+}$ mice produced barely detectable a-wave responses that were greatly desensitized, by >3 log units. Over the following 90 min of dark adaptation, photoresponses in both control and PP2A-deficient rods gradually recovered (Fig. 3*A*). The recovery of the averaged maximal ERG a-wave amplitude to a saturating flash intensity (A_{max}) in control rods could be described by a single-exponential function with a time constant of 18.8 ± 2.0 min (from 14 eyes), and its final level 90 min after the bleach was ~93% of its prebleach dark-adapted value (Fig. 3*B*, black symbols). Remarkably, although PP2A-deficient rods also demonstrated robust recovery after the bleach, the rate of their rod dark adaptation (28.4 ± 2.8 min, from 14 eyes) was significantly slower (Fig. 3*B*, red symbols) than that of control rods. A similar suppression of dark adaptation was observed in the recovery of rod-driven ERG a-wave sensitivity (S_f) following the same bleach (Fig. 3*C*). In these experiments, S_f is defined as the ratio of the dim flash response amplitude and its flash strength, and then normalized by the corresponding dark-adapted A_{max}. These results clearly demonstrate that deletion of PP2A substantially delays the recovery of rod function after exposure to bright light. We conclude that PP2A is required for efficient dark adaptation of rods. Although our recordings were limited by the anesthetic to 90 min and the recovery did not reach 100%, likely due to the partial inhibition of pigment regeneration by anesthetics (36), the trend in the recovery of *Ppp2ca*$^{f/f}$ *iCre75*$^{+}$ mice indicated that they would eventually reach the same final level of ERG a-wave maximal amplitude and sensitivity as their control counterparts. This concept is consistent with the comparable sensitivities of control and PP2A-deficient rods after overnight dark adaptation, as measured by either single-cell (Fig. 2*C*) or ERG (Fig. 3*A*) recordings.

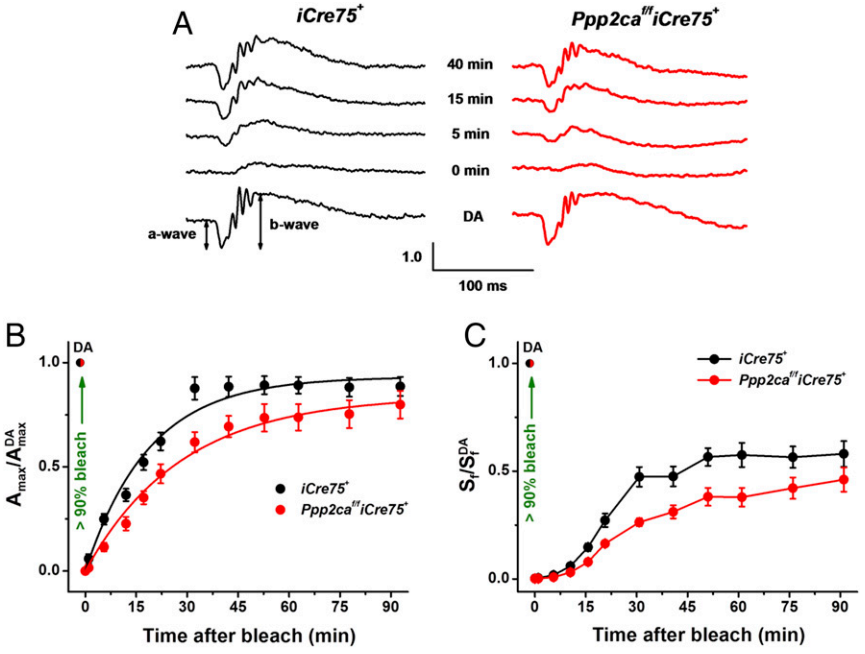

Fig. 3. Suppressed rod dark adaptation in rod-specific PP2A-Cα knockout mice. (*A*) Representative scotopic ERG responses in the dark [dark-adapted (DA), *Bottom*] and at indicated time points after bleaching >90% of the rod pigment in *iCre75*$^{+}$ control (*Left*) and *Ppp2ca*$^{f/f}$ *iCre75*$^{+}$ (*Right*) mice. For each time point, A_{max} values were normalized to their corresponding A_{max}^{DA} value. (*B*) Recovery of scotopic ERG maximal a-wave amplitudes (A_{max}; mean ± SEM) after bleaching >90% of rhodopsin in *iCre75*$^{+}$ control (n = 14) and *Ppp2ca*$^{f/f}$ *iCre75*$^{+}$ (n = 14) mice. Bleaching was achieved by a 35-s illumination with bright 520-nm LED light at time 0. Averaged data points were fitted with single-exponential functions, yielding time constants of 18.8 ± 2.0 and 28.4 ± 2.8 min for control and PP2A-deficient mice, respectively. Final levels of response recovery by 90-min postbleach determined from exponential fits were 93% (*iCre75*$^{+}$) and 81% (*Ppp2ca*$^{f/f}$ *iCre75*$^{+}$). Two-way repeated-measures ANOVA showed overall significant effect of genotype [$F_{(1,312)} = 8.6$; P = 0.007]. (*C*) Recovery of scotopic ERG a-wave flash sensitivity (S_f; mean ± SEM) after bleaching >90% of rod pigment in *iCre75*$^{+}$ control (n = 14) and *Ppp2ca*$^{f/f}$ *iCre75*$^{+}$ (n = 14) mice. Animals and experimental conditions were the same as in *B*. Two-way repeated-measures ANOVA showed overall significant effect of genotype [$F_{(1,312)} = 10.2$; P = 0.004].

Compromised Rhodopsin Dephosphorylation and Chromophore Recycling in Mice with Rod-Specific Ablation of PP2A-Cα. The importance of PP2A for the timely dark adaptation of rods raised the obvious possibility that this enzyme can dephosphorylate their pigment in vivo. To quantify the reversible rhodopsin phosphorylation in mouse rods, we used an assay based on a combination of rhodopsin cleavages to obtain its C-terminal peptides (unphosphorylated or phosphorylated) by reversed-phase HPLC and tandem mass spectrometry (MS/MS) developed previously (37).

We found that both control and PP2A-deficient rods of animals dark-adapted overnight contained predominantly unphosphorylated rhodopsin, along with ∼5% of monophosphorylated pigment (Fig. 4*A*). Notably, there was no difference in the level of phosphorylation in dark-adapted control and PP2A-deficient rods. This result, together with the finding that rod sensitivity in dark-adapted *Ppp2ca*$^{f/f}$ *iCre75*$^{+}$ mice is normal, suggest that rhodopsin dephosphorylation can proceed even in the absence of PP2A-Cα such that rhodopsin in PP2A-deficient rods becomes dephosphorylated after overnight dark adaptation. To determine whether PP2A plays a role in this process, we directly examined the kinetics of rhodopsin dephosphorylation. A few seconds after a 2-min exposure of control *iCre75*$^{+}$ mice to bright light bleaching essentially all of the pigment, phosphorylation by GRK1 produced ∼50% of monophosphorylated (Ser^{343}) and double-phosphorylated (Ser^{343} and Ser^{338}) rhodopsin. The fraction of double-phosphorylated rhodopsin was ∼20% of the total phosphorylated pigment, and triple- or higher-order pigment phosphorylations were negligible under our experimental conditions. As expected, following 3 h of dark adaptation, the fraction of light-generated phosphorylated rhodopsin in control mice decreased substantially and returned to baseline (Fig. 4*A*, black symbols). Thus, rhodopsin was dephosphorylated efficiently in control mice, resetting rods back to their dark-adapted prebleached state. Notably, gradual rhodopsin dephosphorylation in vivo was also observed in PP2A-deficient mice. However, the onset of this process was substantially delayed in the absence of PP2A so that rhodopsin phosphorylation continued to rise and peaked at 30 min after the bleach, reaching a level significantly higher than that in control rods (Fig. 4*A*, red symbols). Subsequent dephosphorylation was also greatly delayed so that even 2 h after the bleach, the level of rhodopsin phosphorylation in *Ppp2ca*$^{f/f}$ *iCre75*$^{+}$ mice remained higher than the peak level in *iCre75*$^{+}$ controls. In contrast, rhodopsin had been largely dephosphorylated in control rods at that time point. Thus, ablation of PP2A from rods dramatically suppressed the dephosphorylation of their visual pigment, demonstrating that PP2A plays a key role in rhodopsin dephosphorylation. However, rhodopsin dephosphorylation was still clearly ongoing in *Ppp2ca*$^{f/f}$ *iCre75*$^{+}$ mice, suggesting that this process can also be driven, albeit more slowly, by alternative means.

To determine whether slower rhodopsin dephosphorylation in PP2A-Cα–deficient rods affects the recycling of visual chromophore and the regeneration of rod pigment, we quantified the levels of visual cycle retinoids in whole mouse eyes by HPLC, first in the dark and then at several time points after a >90% rod pigment bleach. Importantly, the same animals and bleaching conditions used for the rhodopsin phosphorylation analysis described above were employed in this experiment (one eye being used for each of the two measurements). As expected, photoactivation of rhodopsin in control mice immediately converted its chromophore from 11-*cis*-retinal to the all-*trans*- configuration, causing substantial accumulation of all-*trans*-retinal at the first time point after the bleach (Fig. 4*B*, black symbols). After the decay of photoactivated rhodopsin and the release of all-*trans*-retinal, it was rapidly reduced to all-*trans*-retinol, which also showed a statistically significant increase right after the bleach (Fig. 4*C*, black symbols) compared with controls. The unaccounted difference (150 pmol of retinoid) between the levels of bleached 11-*cis*-retinal and the sum of all-*trans*-retinol and all-*trans*-retinal can be attributed to levels of retinyl esters formed during the bleaching, extraction, and processing of the samples. It is unlikely that such esters would affect our findings as their formation occurs in RPE cells, where PP2A expression is not altered, and only after the release of all-*trans*-retinol from photoreceptors. Eventually, 11-*cis*-retinal levels were restored in control

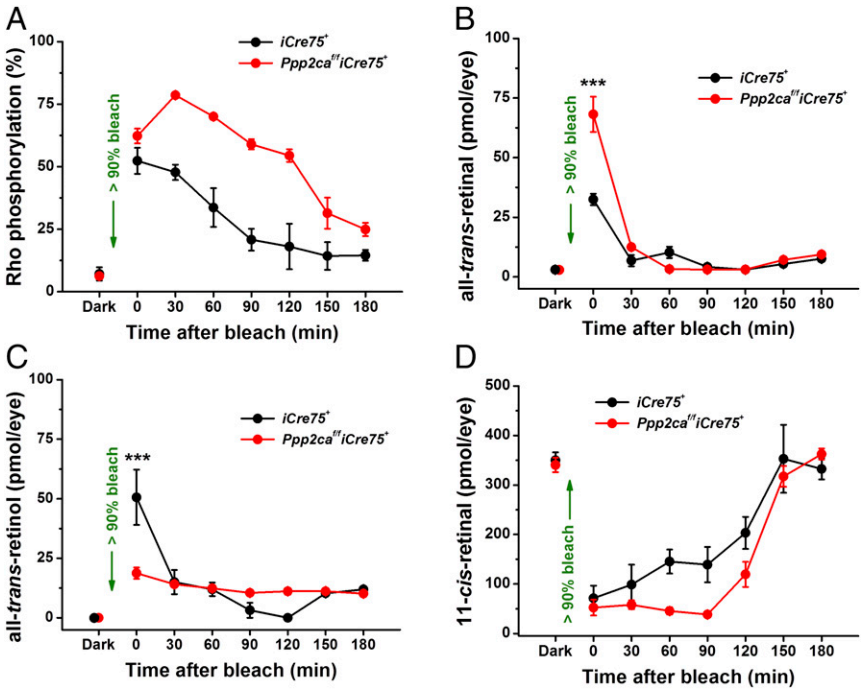

Fig. 4. Compromised rhodopsin dephosphorylation and visual cycle in rod-specific PP2A-Cα knockout mice. (*A*) Total rhodopsin phosphorylation levels (mean ± SEM) in the dark and at different times after >90% pigment bleach in whole eyes of *iCre75*$^{+}$ control (n = 5 for each time point) and *Ppp2ca*$^{f/f}$ *iCre75*$^{+}$ (n = 5 for each time point) mice. Live animals were exposed to white light (5,000 lx) for 2 min at time 0. Basal (prebleached) levels of rhodopsin phosphorylation were ∼5%. Two-way repeated-measures ANOVA showed overall significant effect of genotype [$F_{(1,36)} = 110.1$; $P < 0.001$]. (*B*) Light-induced changes of all-*trans*-retinal amounts (mean ± SEM) in whole eyes of *iCre75*$^{+}$ control (n = 5 for each time point) and *Ppp2ca*$^{f/f}$ *iCre75*$^{+}$ (n = 5 for each time point) mice. Animals and bleaching conditions were the same as in *A*. Two-way repeated-measures ANOVA showed overall significant effect of genotype [$F_{(1,36)} = 20.3$; $P = 0.004$]. Bonferroni post hoc analysis demonstrated that only first postbleach data at 0 min was significantly different (***$P < 0.001$). (*C*) Light-induced changes of all-*trans*-retinol levels (mean ± SEM) in whole eyes of *iCre75*$^{+}$ control (n = 5 for each time point) and *Ppp2ca*$^{f/f}$ *iCre75*$^{+}$ (n = 5 for each time point) mice. Animals and bleaching conditions were the same as in *A*. Two-way repeated-measures ANOVA did not reveal overall significant effect of genotype [$F_{(1,36)} = 3.0$; $P = 0.132$]. Bonferroni post hoc analysis demonstrated that the first postbleach data point was significantly different between control and mutant mice (***$P < 0.001$). All "between" and "within" genotype post hoc comparisons of the data at 60 min postbleach and after showed no statistical difference. (*D*) Regeneration of 11-*cis*-retinal in whole eyes of *iCre75*$^{+}$ control (n = 5 for each time point) and *Ppp2ca*$^{f/f}$ *iCre75*$^{+}$ (n = 5 for each time point) mice. Animals and bleaching conditions were the same as in *A*. Data represent mean ± SEM. Two-way repeated-measures ANOVA showed overall significant effect of genotype [$F_{(1,36)} = 14.0$; $P = 0.01$].

bleached eyes, as it was recycled by the RPE (Fig. 4*D*, black symbols). Notably, the recycling of 11-*cis*-retinal was substantially delayed in the absence of PP2A-Cα, but it still eventually reached its dark levels (Fig. 4*D*, red symbols). The compromised regeneration of visual chromophore was accompanied by very slow production of all-*trans*-retinol in *Ppp2ca*$^{f/f}$ *iCre75*$^{+}$ mice (Fig. 4*C*, red symbols). Instead, in mutant retinas, we observed a statistically significant (compared with controls) buildup of its immediate precursor, all-*trans*-retinal, at the early postbleach times (Fig. 4*B*, red symbols). Thus, the conversion of all-*trans*-retinal to all-*trans*-retinol in rods appeared suppressed in the absence of PP2A, causing a delay in the recycling of chromophore and, ultimately, in the regeneration of rod visual pigment.

Taken together, these findings clearly demonstrate that PP2A serves as rhodopsin phosphatase in vivo, so that ablation of its major catalytic subunit results in compromised pigment dephosphorylation, delayed recycling of visual chromophore, and slower pigment regeneration. Equally important, these data demonstrate the existence of additional phosphatase(s) capable of dephosphorylating rhodopsin in the absence of PP2A-Cα.

Phosducin Dephosphorylation in Mice with Rod-Specific Ablation of PP2A-Cα. In addition to rhodopsin dephosphorylation, PP2A has also been proposed to be involved in the dephosphorylation of another abundant phosphoprotein, phosducin (Pdc). To determine whether PP2A is an innate Pdc phosphatase, we compared the kinetics of light-dependent Pdc phosphorylation in *Ppp2ca*$^{f/f}$ *iCre75*$^{+}$ mice and control *iCre75*$^{+}$ animals. Phosphorylation of serine 71 (Fig. 5*A*), a prominent Pdc phosphorylation site (28, 38), was monitored by Western blotting with a previously characterized phosphospecific Pdc71p antibody (39). In the eye, Pdc is predominantly expressed in rod and cone photoreceptors of the retina and is virtually undetectable in other cell types. Thus, probing whole-eye extracts revealed the phosphorylation status of Pdc in retinal photoreceptors, specifically in the dominating rods.

The kinetics of Pdc dephosphorylation could not be monitored directly because the tissue collection protocol was longer than the ∼2 min required for complete dephosphorylation of Pdc in vivo (39). As an alternative, we measured the kinetics of Pdc phosphorylation in the dark, which is substantially slower. The rationale was that the addition of phosphate groups would occur faster in the absence of PP2A-Cα, which removes these groups. In both *Ppp2ca*$^{f/f}$ *iCre75*$^{+}$ and *iCre75*$^{+}$ mice, Pdc underwent robust dephosphorylation during the 10 min of exposure to dim 10-lx light (Fig. 5*B*, time point 0 min). Within 10 min of subsequent dark adaptation, Pdc regained its phosphorylated state (Fig. 5*B*, time points 10 and 30 min). No statistically significant difference in the kinetics of Pdc phosphorylation in control and PP2A-deficient rods was observed at any time. This result is in contrast to the predicted increase in Pdc phosphorylation in the absence of its phosphatase. Finally, the level of Pdc phosphorylation was also comparable in control and PP2A-deficient mice after overnight dark adaptation. Thus, perhaps surprisingly, these results demonstrate that PP2A-Cα is not required for the dephosphorylation of Pdc in retinal rod photoreceptors, leaving the identity of the enzyme responsible for catalyzing this reaction unknown.

Impaired Cone Dark Adaptation in Mice with Cone-Specific Ablation of PP2A-Cα. Phosphorylation of photoactivated visual pigment also takes place in vertebrate cones (40), but the enzyme that subsequently dephosphorylates cone pigments has not been identified. It also is unknown whether cone pigment dephosphorylation plays a role in regulating the function of mammalian cones by affecting their pigment regeneration or dark adaptation. Our in situ mRNA hybridization analysis demonstrated the expression of the Cα-subunit of PP2A in cone-like photoreceptors of *Nrl*$^{-/-}$ mouse retina, suggesting that PP2A is present in mouse cones as well (Fig. 6*A*). Also consistent with PP2A expression in cones is the residual expression of PP2A observed in a small fraction of photoreceptors in *Ppp2ca*$^{f/f}$ *iCre75*$^{+}$ mice (Fig. 1 *B* and *D*). Thus, to investigate the potential role of PP2A in cone function, we crossed our PP2A-floxed mice with the transgenic *HRGP-Cre*$^{+}$ line expressing *Cre* recombinase selectively in cones (41) to generate cone-specific PP2A conditional knockout (*Ppp2ca*$^{f/f}$ *HRGP-Cre*$^{+}$) mice. To facilitate recordings specifically from cones, mice were derived on a *Gnat1*$^{-/-}$ background that eliminates the rod component of the light response without affecting cone morphology or function (42).

Because the bulk of immunohistochemical PP2A staining in the photoreceptor layer originates in rod cells, it is rather challenging to confirm the elimination of PP2A protein from the cones, which represent only a minor (∼3%) fraction of photoreceptors in mouse retina (43). However, as the rod results above demonstrate, conditional knockout of PP2A-Cα by *Cre*-mediated recombination effectively ablates PP2A-Cα expression. Therefore, we sought to confirm the robust expression of *Cre* recombinase in the cones of *Ppp2ca*$^{f/f}$ *HRGP-Cre*$^{+}$ mice. Cones were identified by immunolabeling with cone arrestin antibody (Fig. 6*B*; see *Materials and Methods* for details). Analysis of the expression of *Cre* recombinase in *Ppp2ca*$^{f/f}$ *HRGP-Cre*$^{+}$ mouse retina revealed immunolabeling selectively in cones at the top of the outer nuclear layer (Fig. 6*B*, *Right*), indicating that *Cre* is indeed expressed in their cone nuclei. This result, together with the robust functional phenotype of *Ppp2ca*$^{f/f}$ *HRGP-Cre*$^{+}$ mice described below, demonstrate the successful ablation of PP2A-Cα in their cones.

To address the possible role of PP2A in cone phototransduction and dark adaptation, we performed a series of physiological experiments in both isolated retinas and live animals. The analysis was limited to M-opsin–expressing cones, which can be selectively stimulated with visible green light. ERG recordings from isolated retinas in the presence of postsynaptic blockers revealed that, under dark-adapted conditions, the flash responses of M-cones from *Ppp2ca*$^{f/f}$ *HRGP-Cre*$^{+}$ mice had amplitudes (Fig. 6 *C* and *D*), sensitivity (Fig. 6*E*), and kinetics (Fig. 6*F*) comparable to those of M-cone responses

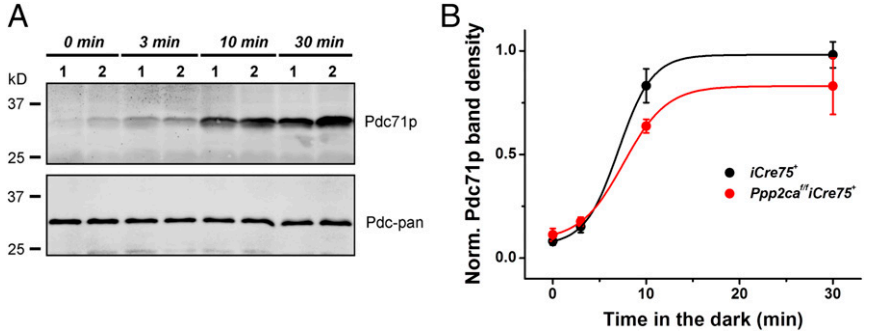

Fig. 5. Normal phosducin phosphorylation in rod-specific PP2A-Cα knockout mice. (*A*) Monitoring phosphorylation status of phosducin in retinal photoreceptors by Western blotting. Dark-adapted mice were exposed to white light (10 lx) for 10 min, and then returned to darkness. At times indicated (0, 3, 10, 30 min), mice were killed, and their eyes were collected and flash-frozen. Levels of phosphorylated phosducin in whole-eye extracts were determined by Western blotting with Pdc71p antibody. Total levels of phosducin were determined with Pdc-pan antibody after diluting the original extracts 100 times. 1, Control *iCre75*$^{+}$ sample; 2, *Ppp2ca*$^{f/f}$ *iCre75*$^{+}$ sample. (*B*) Kinetics of Pdc phosphorylation upon the onset of darkness. Fluorescence values of Pdc71p bands were divided by those of the corresponding Pdc-pan band and plotted as a function of the time mice spent in the dark (mean ± SEM; $n = 4$, for both control and mutant lines). Two-way repeated-measures ANOVA did not reveal overall significant effect of genotype [$F_{(1,28)} = 1.6$; $P = 0.23$]. Data were fitted with a sigmoidal curve for illustration.

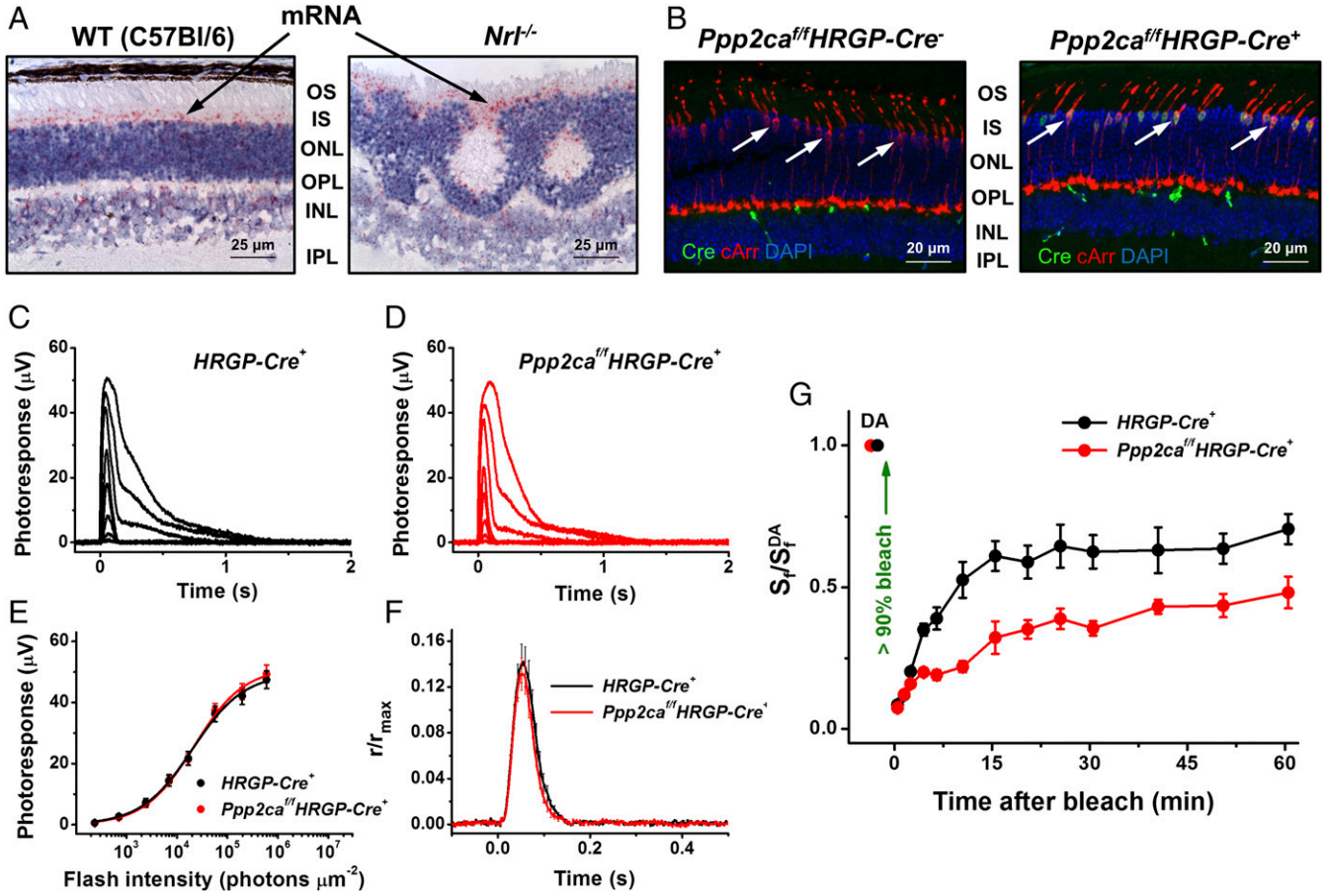

Fig. 6. Morphological and functional characterization of cone-specific PP2A-Cα knockout mice. (*A*) Expression of PP2A-Cα in mouse cones. In situ hybridization of 2-mo-old WT (C57BL/6) and $Nrl^{-/-}$ mouse retinas with a PP2A-Cα probe (RNAscope, ACD). INL, inner nuclear layer; IPL, inner plexiform layer; IS, inner segments; ONL, outer nuclear layer; OPL, outer plexiform layer; OS, outer segments. (Scale bar, 25 μm.) (*B*) Cone-specific expression of *Cre* recombinase in *Ppp2ca*$^{f/f}$*Gnat1*$^{-/-}$*HRGP-Cre*$^{+}$ mice. Immunostaining of littermate *Ppp2ca*$^{f/f}$*Gnat1*$^{-/-}$*HRGP-Cre*$^{-}$ control and *Ppp2ca*$^{f/f}$*Gnat1*$^{-/-}$*HRGP-Cre*$^{+}$ mouse retinas with anti-*Cre* (green) and anti-cone arrestin (red) antibodies. Cell nuclei were stained with DAPI (blue). Arrows show positions of cone nuclei. (Scale bar, 20 μm.) (*C*) Representative family of transretinal cone ERG responses from *HRGP-Cre*$^{+}$ control mouse retinas. Test flashes of 505-nm light with intensities of 235, 705, 2.4×10^3, 7.0×10^3, 1.7×10^4, 5.7×10^4, 2.0×10^5, and 6.0×10^5 photons·μm^{-2} were delivered at time 0. (*D*) Representative family of transretinal cone ERG responses from *Ppp2ca*$^{f/f}$ *HRGP-Cre*$^{+}$ mouse retinas. Intensities of test flashes of 505-nm light were the same as in *C*. (*E*) Averaged cone intensity–response functions (mean ± SEM) for *HRGP-Cre*$^{+}$ control ($n = 20$) and *Ppp2ca*$^{f/f}$ *HRGP-Cre*$^{+}$ ($n = 15$) mice. Data were fitted with hyperbolic Naka–Rushton functions that yielded half-saturating intensities ($I_{1/2}$) of 2.0×10^4 and 2.2×10^4 photons·μm^{-2} for control and PP2A-deficient cones, respectively. (*F*) Kinetics of cone phototransduction activation and inactivation in *HRGP-Cre*$^{+}$ control ($n = 20$) and *Ppp2ca*$^{f/f}$ *HRGP-Cre*$^{+}$ ($n = 15$) retinas. Population-averaged dim flash responses to light intensity of 2.4×10^3 photons·μm^{-2} were normalized to their respective maximal responses in the dark (R_{max}). Error bars indicate SEM. (*G*) Delayed cone dark adaptation in cone-specific PP2A-Cα knockout mice in vivo. Recovery of cone ERG b-wave flash sensitivity (S_f; mean ± SEM) after bleaching >90% of cone visual pigment in *HRGP-Cre*$^{+}$ control ($n = 10$) and *Ppp2ca*$^{f/f}$ *HRGP-Cre*$^{+}$ ($n = 12$) mice. Bleaching was achieved by a 35-s illumination with bright 520-nm LED light at time 0. Final levels of sensitivity recovery at 60 min postbleach were 70% (*HRGP-Cre*$^{+}$) and 54% (*Ppp2ca*$^{f/f}$ *HRGP-Cre*$^{+}$). Two-way repeated-measures ANOVA showed overall significant effect of genotype [$F_{(1,260)} = 35.7$; $P < 0.001$].

from control *HRGP-Cre*$^{+}$ mice. These results demonstrate that, as in the case of rods, deletion of PP2A-Cα in cones did not produce adverse effects on their cell number, overall health, or phototransduction in dark-adapted conditions. However, ERG recordings from live animals showed that M-cone dark adaptation (estimated from the recovery of cone ERG b-wave flash sensitivity) after a near-complete bleaching of cone visual pigment was severely suppressed in *Ppp2ca*$^{f/f}$ *HRGP-Cre*$^{+}$ mice (Fig. 6*G*). These findings indicate that, similar to rods, PP2A is the pigment phosphatase in mammalian M-cones as well, and its deletion significantly compromises the dark adaptation of mouse cone photoreceptors.

Discussion

Reversible phosphorylation is one of the key cellular mechanisms allowing recurrent GPCR signaling. The state of phosphorylation, which regulates the activity of many GPCRs, is controlled by two enzymatic groups, protein kinases and phosphatases (44–46). In retinal photoreceptor neurons, continuous detection of light requires the timely shutoff of their highly specialized GPCRs, visual pigments, and the rapid inactivation of their phototransduction cascade. Similar to other G-protein cascades, partial inactivation of visual pigment is initiated by the multiple phosphorylation of its C terminus that in rods is mediated by GRK1 (10, 47). This phosphorylation is regulated by calcium via the calcium-binding protein recoverin in both rods (48) and cones (49). Subsequent binding of arrestin fully inactivates the pigment and results in the eventual termination of the light response (12, 13).

The role of visual pigment phosphorylation has been well characterized. Its blockade by either deletion of GRK1 (11), truncation of the opsin C terminus containing the targeted Ser/Thr residues (50), or mutation of these residues themselves (51), greatly delays the shutoff of the light response and causes persistent phototransduction activity and light-dependent retinal degeneration (11). In addition, the timely phosphorylation of rhodopsin controls the reproducibility of rod responses to light (52, 53). Notably, phosphorylated rhodopsin activates the phototransduction cascade with

reduced efficiency (32) and lowers the sensitivity of mammalian rods (54). Thus, a critical but often overlooked step in resetting the ground state of the visual pigment is its dephosphorylation needed to fully recover the receptor's ability to repeatedly trigger phototransduction. However, despite the remarkable progress in understanding G-protein signaling in general and phototransduction in particular, the mammalian rod enzyme(s) responsible for catalyzing this reaction in vivo has remained unknown (16). Furthermore, although in vertebrate cones both the decay of photoactivated pigment and its subsequent regeneration with 11-*cis*-retinal (55, 56), as well as their opsin dephosphorylation (40, 57), proceed significantly faster than in rods, the identity of the cone pigment phosphatase is also unknown.

Here, we determined that the ubiquitously expressed enzyme PP2A is the pigment phosphatase in mammalian rods and cones (20, 22, 23) and demonstrated the significance of pigment dephosphorylation in the function of photoreceptors. Based on previous RNA-sequencing analysis, PP2A-Cα mRNA is ∼2.3-fold more abundant than PP2A-Cβ mRNA in wild-type mouse retinas (58). This finding suggests that, as in most other tissues, PP2A-Cα is the primary PP2A catalytic subunit in mammalian photoreceptors. Thus, we generated two unique conditional knockout mouse lines, with either rod- or cone-specific ablation of PP2A-Cα.

We show that PP2A-Cα is indeed expressed in both photoreceptor types (Figs. 1 *B* and *D* and 6*A*). Despite the ubiquitous nature of PP2A, its ablation from mouse rods or cones does not affect their overall morphology (Figs. 1*E* and 6*B*) or signaling efficiency (Figs. 2 and 6 *C*–*F*). However, in both rods and cones, the deletion of PP2A-Cα suppresses their dark adaptation following a nearly complete pigment bleach (Figs. 3 and 6*G*). In the case of rods, this delay is associated with compromised pigment dephosphorylation (Fig. 4*A*). Moreover, the lack of PP2A-mediated rhodopsin dephosphorylation significantly delays the recycling of 11-*cis*-retinal visual chromophore (Fig. 4*D*). This process begins with the release of the photoisomerized chromophore, all-*trans*-retinal, from photoreceptors, followed by its conversion back to the 11-*cis*- form in the RPE (for both rods and cones) or in Müller cells (for cones only) (59–61). The recycled chromophore then is returned to photoreceptors, where it combines with apo-opsin to regenerate the visual pigment. Currently, it is not possible to biochemically characterize the recycling of visual chromophore in mouse cones due to their scarcity in the retina. However, the substantial delay of M-cone dark adaptation in the absence of PP2A-Cα indicates that the PP2A-driven dephosphorylation of opsin is a critical step in the dark adaptation not only in mammalian rods, but in cones as well. However, we also found that the visual pigment eventually is reset to its ground (dephosphorylated) state even in the absence of PP2A. Thus, our results also suggest the existence of additional mechanisms for dephosphorylation of visual pigments (e.g., by PP2A-Cβ or other cellular phosphatases).

One important issue related to dark adaptation that remains to be resolved is whether visual opsin is dephosphorylated before or after its recombination with 11-*cis*-retinal, that is, what is the rate-limiting step in this process? Previous studies have shown that, for mouse rhodopsin, the rate of phosphate removal from the more proximally located Ser^{334} is slower than dephosphorylation of the more distal Ser^{338} and Ser^{343} residues (62), and that this correlates with the overall rate of dark adaptation of rods in vivo (63). The latter study also attempted to determine whether recycling of visual chromophore through the RPE visual cycle and its subsequent delivery to rods is a prerequisite for dephosphorylation of rod opsin. The authors measured the rate of rhodopsin dephosphorylation in mice lacking the RPE cellular retinaldehyde-binding protein (CRALBP), which results in substantially slower recycling of chromophore by the RPE visual cycle (64). Rhodopsin dephosphorylation in these mice was found to be normal, suggesting that dephosphorylation is independent of the recombination of apo-opsin with 11-*cis*-retinal (63). This conclusion is also supported by more recent work on purified carp rod and cone outer segment membranes in which dephosphorylation of rod or cone opsins was unaffected by the regeneration of both pigments, as measured by an excess of 11-*cis*-retinal (ref. 57; see also ref. 65). Arrestin binding also inhibits rhodopsin dephosphorylation (66, 67), implying that the dephosphorylation step most likely occurs following the thermal decay of photoactive rhodopsin. Moreover, under prolonged bright illumination, the subsequent recovery of rod current in the dark correlates closely with both rhodopsin regeneration and its biphasic dephosphorylation (68), thus supporting the idea that regeneration of rod pigment with 11-*cis*-retinal is needed to release bound arrestin, thereby allowing the dephosphorylation reaction to occur.

While informative, these studies do not address the functional significance of visual pigment dephosphorylation in photoreceptor cells. Instead, our approach of genetically ablating a candidate pigment phosphatase revealed the role of this process in rod and cone dark adaptation. One of two mechanisms could cause the delay in photoreceptor dark adaptation observed in PP2A-Cα knockout mice. First, pigment regeneration could take place normally in the absence of PP2A-Cα, but the residual pigment phosphorylation could suppress its full capacity to activate the phototransduction cascade (54). Alternatively, if dephosphorylation is required for the efficient decay or eventual regeneration of visual pigment, suppressed dephosphorylation in the absence of PP2A could directly affect the rate of pigment regeneration in vivo. Our biochemical analysis of PP2A-deficient rods allowed discrimination between these two scenarios. The present results clearly show that the normally rapid conversion of all-*trans*-retinal to all-*trans*-retinol (56, 69) is suppressed in PP2A-deficient rods (Fig. 4 *B* and *C*), and this results in slower recycling of 11-*cis*-retinal by the RPE visual cycle (Fig. 4*D*) and delayed rod dark adaptation (Fig. 3). Although direct regulation of enzymes involved in rod visual cycle or generation of retinol dehydrogenase cofactor NADPH cannot be ruled out, the simplest explanation for these findings is that the suppression of visual pigment dephosphorylation in PP2A-deficient rods delays the decay of photoactivated pigment into apo-opsin and all-*trans*-retinal. Consistent with this notion, a recent study found that the decay of photoactivated mouse rhodopsin is accelerated in the absence of rhodopsin phosphorylation by GRK1 (70). Thus, the present results suggest that the timely dephosphorylation of the visual pigment is required for the rapid release of spent chromophore from opsin. This represents a unique mechanism of regulation of the visual cycle by PP2A that ultimately affects the kinetics of dark adaptation of rod and cone photoreceptors.

Previous biochemical work has suggested that the dephosphorylation of phosducin (a modulator of light-dependent transducin translocation) is another target of PP2A in photoreceptors (23, 28). However, we found that deletion of PP2A-Cα from rods does not abolish dephosphorylation of phosducin upon light exposure and has no significant effect on the kinetics of phosducin phosphorylation in the dark (Fig. 5). Thus, the balance between phosphorylation and dephosphorylation of phosducin was not affected in the absence of PP2A-Cα. This surprising result suggests that another, yet-unidentified enzyme is responsible for phosducin dephosphorylation in vivo. Future studies should help to identify the responsible phosphatase and ultimately determine the functional significance of the phosphorylation state of phosducin.

In summary, this study establishes a role for PP2A as the visual pigment phosphatase that resets the ground state of rod and cone pigments after their photoactivation. As visual pigments represent prototypical G-protein–coupled cellular receptors, this work sheds light on the general mechanism of recycling of activated GPCRs, a process essential for their resensitization and continuous signaling.

Materials and Methods

Generation of PP2A Conditional Knockout Mouse Lines. All experiments were approved by the Washington University Animal Studies Committee and the Case Western Reserve University Animal Care Committee. Unless otherwise specified, all control and experimental mice of either sex were used at 2–5 mo of age. *Ppp2ca*-floxed mice were generated by recombineering methods.

Following successful germline transmission and FLPo-mediated elimination of the *Neo* cassette, both confirmed by PCR, they were bred to homozygosity. For rod-specific elimination of the PP2A-Cα, *Ppp2ca*-floxed mice were bred with *rhodopsin-Cre* (*iCre75*$^{+}$) mice (30) and finally inbred to produce homozygous *Ppp2ca*$^{f/f}$*iCre75*$^{+}$ animals. For all rod-related experiments, littermate *Ppp2ca*$^{+/+}$*iCre75*$^{+}$ mice were used as controls. To delete PP2A-Cα exclusively in M-cones, *Ppp2ca*-floxed mice were bred with human red/green pigment gene promoter *Cre* (*HRGP-Cre*$^{+}$) mice that express *Cre* recombinase selectively in cones (41). These animals were further bred with rod transducin α-subunit knockout (*Gnat1*$^{-/-}$) mice, which lack functional rod phototransduction (42). The resulting *Ppp2ca*$^{f/f}$*Gnat1*$^{-/-}$*HRGP-Cre*$^{+}$ mice were used for all cone-related electrophysiological experiments, with *Ppp2ca*$^{f/f}$*Gnat1*$^{-/-}$*HRGP-Cre*$^{-}$ or *Ppp2ca*$^{+/+}$*Gnat1*$^{-/-}$*HRGP-Cre*$^{+}$ mice employed as controls.

All PP2A mice were homozygous for the Met-450 isoform of RPE65 (71) and were free of the *Crb1/rd8* mutation (72). *Nrl*$^{-/-}$ mice used to detect PP2A-Cα mRNA in cones have been described earlier (73). Housing conditions, detailed procedures for generation of PP2A conditional knockout mouse lines, and genotyping are described in *SI Materials and Methods*.

Light Microscopy. Five-month-old mice were killed by CO_2 asphyxiation, and their eyes were enucleated and immersion-fixed for 24 h in PBS (pH 7.4) containing 2% glutaraldehyde and 2% paraformaldehyde, at 4 °C. After dehydration, eyecups were embedded in an EPON-Araldite mixture, and 1-μm sections were cut dorsal to ventral through the optic nerve and stained with hematoxylin and eosin (H&E). Images were acquired from the central retina near the optic nerve head.

Antibodies and Immunohistochemistry. After removal of the cornea and lens, the remaining mouse eyecup was fixed in freshly prepared 4% paraformaldehyde in 0.1 M PBS at pH 7.4 for 2 h at 4 °C. Details on the protocol and antibodies used are described in *SI Materials and Methods*.

In Situ mRNA Hybridization. Expression of PP2A-Cα mRNA in mouse rods and cones was visualized by in situ mRNA hybridization in control and *Nrl*$^{-/-}$ retinas, respectively. Mouse *Ppp2ca* target oligonucleotide probes for manual assays were designed and produced by Advanced Cell Diagnostics. The RNAscope 2.5 HD Red Assay Kit (ACD) was used for in situ mRNA hybridization, and all procedures were carried out according to the manufacturer's RNAscope Technology protocol (31).

qRT-PCR. Mouse retinas were promptly homogenized and passed through a QIAShredder column (Qiagen) to further homogenize the eye tissues. Total RNA was then purified with the RNeasy Mini Kit (Qiagen) along with on-column DNase treatment (Qiagen) as per the manufacturer's directions. Total RNA from mouse retinas was reverse-transcribed with a high-capacity cDNA reverse transcription kit (Applied Biosystems) and used as a template for a qRT-PCR with TaqMan Gene Expression Assays (Applied Biosystems) following the manufacturer's instructions. Details on the protocol and probes used are described in *SI Materials and Methods*.

Rhodopsin Phosphorylation Analysis. The method for the separation of rhodopsin phospho- and nonphosphopeptides by reversed-phase HPLC in combination with MS/MS has been described previously (37, 63). Dark-adapted or light-exposed (5,000-lx white light, 2 min) mice were killed by cervical dislocation at specified postbleach times, and their right eyes were immediately removed, flash-frozen in liquid N_2, and homogenized in 700 μL of 7 M urea in 10 mM Tris·HCl, pH 7.4. All procedures for separation and quantification of rhodopsin phosphopeptides are described in *SI Materials and Methods*.

Quantification of Visual Cycle Retinoids. After pigment bleaching and the killing of animals as described in a previous section, left eyes of the same dark-adapted mice were flash-frozen in liquid N_2 and thoroughly homogenized in 1 mL of ice-cold buffer containing 50 mM Mops, pH 7.0, 10 mM NH_2OH, and 50% ethanol. Retinoids were identified and quantified by comparison with authentic standards, as described previously (74). Details on the quantification of retinoids are provided in *SI Materials and Methods*.

Single-Cell Rod Suction Electrode Recordings. Control and rod-specific PP2A mutant animals were dark-adapted overnight and killed by CO_2 asphyxiation, and their retinas were removed under infrared illumination, chopped into small pieces, and transferred into a perfusion chamber located on the stage of an inverted microscope. A single rod outer segment was drawn into a glass microelectrode filled with Locke's physiological solution, for recordings. Test flashes (20 ms) of calibrated 500-nm light were delivered by an optical bench. Details on the recordings and the data analysis are described in *SI Materials and Methods*.

Ex Vivo Cone Recordings from Isolated Mouse Retinas. Control and rod-specific PP2A mutant mice were dark-adapted overnight and killed by CO_2 asphyxiation, and the whole retina was removed from each mouse eyecup under infrared illumination and stored in oxygenated aqueous L15 (13.6 mg/mL, pH 7.4) solution (Millipore Sigma) containing 0.1% BSA, at room temperature (RT). The retina was oriented with its photoreceptor side up and placed into a perfusion chamber (75) between two electrodes connected to a differential amplifier. The specimen was perfused with Locke's solution supplemented with 1.5 mM L-glutamate and 40 μM DL-2-amino-4-phosphonobutyric acid to block postsynaptic components of the photoresponse (76), and with 70 μM $BaCl_2$ to suppress the slow glial PIII component (77). The perfusion solution was continuously bubbled with a 95% O_2/5% CO_2 mixture and heated to 36–37 °C. Light stimulation was applied in 20-ms test flashes of calibrated 505-nm LED light. Other details are provided in *SI Materials and Methods*.

In Vivo ERG. Dark-adapted mice were anesthetized with an i.p. injection of a mixture of ketamine (100 mg/kg) and xylazine (20 mg/kg). Pupils were dilated with a drop of 1% atropine sulfate. Mouse body temperature was maintained at 37 °C with a heating pad. ERG responses were measured from both eyes by contact corneal electrodes held in place by a drop of Gonak solution (Akorn). Full-field ERGs were recorded with a UTAS BigShot apparatus (LKC Technologies) using Ganzfeld-derived test flashes of calibrated green 530-nm LED light. Details on the recordings, dark adaptation test, and data analysis are described in *SI Materials and Methods*.

Statistics. For all experiments, data were expressed as mean ± SEM and analyzed with the independent two-tailed Student *t* test (using an accepted significance level of $P < 0.05$) or two-way repeated-measures ANOVA (with genotype as main factor and time as repeated measures factor). In the latter case, pairwise comparisons were performed using the Bonferroni post hoc test, and $P < 0.05$ was considered significant.

ACKNOWLEDGMENTS. We are thankful to the V.J.K. and K.P. laboratories for comments on the manuscript. Especially, we thank Drs. Ning Zhang and Jianye Zhang for their help during this study. This work was supported by NIH Grants EY026675 (to V.J.K. and K.P.), EY019312 (to V.J.K.), and EY02687 (Department of Ophthalmology and Visual Sciences, Washington University), and by Research to Prevent Blindness. L.H. is supported by a Swiss National Science Foundation Doc.Mobility Fellowship (P1SKP3_158634). K.P. is John H. Hord Professor of Pharmacology.

1. Okada T, Palczewski K (2001) Crystal structure of rhodopsin: Implications for vision and beyond. *Curr Opin Struct Biol* 11:420–426.
2. Carman CV, Benovic JL (1998) G-protein-coupled receptors: Turn-ons and turn-offs. *Curr Opin Neurobiol* 8:335–344.
3. Lefkowitz RJ (2004) Historical review: A brief history and personal retrospective of seven-transmembrane receptors. *Trends Pharmacol Sci* 25:413–422.
4. Arshavsky VY, Lamb TD, Pugh EN, Jr (2002) G proteins and phototransduction. *Annu Rev Physiol* 64:153–187.
5. Burns ME, Baylor DA (2001) Activation, deactivation, and adaptation in vertebrate photoreceptor cells. *Annu Rev Neurosci* 24:779–805.
6. Hamer RD, Nicholas SC, Tranchina D, Lamb TD, Jarvinen JL (2005) Toward a unified model of vertebrate rod phototransduction. *Vis Neurosci* 22:417–436.
7. Palczewski K (2006) G protein-coupled receptor rhodopsin. *Annu Rev Biochem* 75: 743–767.
8. Hubbard R (1958) Bleaching of rhodopsin by light and by heat. *Nature* 181:1126.
9. Yau K-W (1994) Phototransduction mechanism in retinal rods and cones. The Friedenwald Lecture. *Invest Ophthalmol Vis Sci* 35:9–32.
10. Ohguro H, Palczewski K, Ericsson LH, Walsh KA, Johnson RS (1993) Sequential phosphorylation of rhodopsin at multiple sites. *Biochemistry* 32:5718–5724.
11. Chen CK, et al. (1999) Abnormal photoresponses and light-induced apoptosis in rods lacking rhodopsin kinase. *Proc Natl Acad Sci USA* 96:3718–3722.
12. Wilden U, Hall SW, Kühn H (1986) Phosphodiesterase activation by photoexcited rhodopsin is quenched when rhodopsin is phosphorylated and binds the intrinsic 48-kDa protein of rod outer segments. *Proc Natl Acad Sci USA* 83:1174–1178.
13. Xu J, et al. (1997) Prolonged photoresponses in transgenic mouse rods lacking arrestin. *Nature* 389:505–509.
14. Vinós J, Jalink K, Hardy RW, Britt SG, Zuker CS (1997) A G protein-coupled receptor phosphatase required for rhodopsin function. *Science* 277:687–690.
15. Sherman PM, et al. (1997) Identification and characterization of a conserved family of protein serine/threonine phosphatases homologous to *Drosophila* retinal degeneration C. *Proc Natl Acad Sci USA* 94:11639–11644.
16. Ramulu P, et al. (2001) Normal light response, photoreceptor integrity, and rhodopsin dephosphorylation in mice lacking both protein phosphatases with EF hands (PPEF-1 and PPEF-2). *Mol Cell Biol* 21:8605–8614.

17. Yang SD, Benovic JL, Fong YL, Caron MG, Lefkowitz RJ (1991) Cyclic phosphorylation-dephosphorylation of rhodopsin in retina by protein kinase FA (the activator of ATP. Mg-dependent protein phosphatase). *Biochem Biophys Res Commun* 178:1306–1311.
18. Kutuzov MA, Bennett N (1996) Calcium-activated opsin phosphatase activity in retinal rod outer segments. *Eur J Biochem* 238:613–622.
19. Klumpp S, et al. (1998) Protein phosphatase type-2C isozymes present in vertebrate retinae: Purification, characterization, and localization in photoreceptors. *J Neurosci Res* 51:328–338.
20. Fowles C, Akhtar M, Cohen P (1989) Interplay of phosphorylation and dephosphorylation in vision: Protein phosphatases of bovine rod outer segments. *Biochemistry* 28:9385–9391.
21. King AJ, Andjelkovic N, Hemmings BA, Akhtar M (1994) The phospho-opsin phosphatase from bovine rod outer segments. An insight into the mechanism of stimulation of type-2A protein phosphatase activity by protamine. *Eur J Biochem* 225: 383–394.
22. Palczewski K, Hargrave PA, McDowell JH, Ingebritsen TS (1989) The catalytic subunit of phosphatase 2A dephosphorylates phosphoopsin. *Biochemistry* 28:415–419.
23. Brown BM, Carlson BL, Zhu X, Lolley RN, Craft CM (2002) Light-driven translocation of the protein phosphatase 2A complex regulates light/dark dephosphorylation of phosducin and rhodopsin. *Biochemistry* 41:13526–13538.
24. Vasudevan NT, Mohan ML, Gupta MK, Hussain AK, Naga Prasad SV (2011) Inhibition of protein phosphatase 2A activity by PI3Kγ regulates β-adrenergic receptor function. *Mol Cell* 41:636–648.
25. Evans BJ, et al. (2008) Physical association of GPR54 C-terminal with protein phosphatase 2A. *Biochem Biophys Res Commun* 377:1067–1071.
26. Götz J, Probst A, Ehler E, Hemmings B, Kues W (1998) Delayed embryonic lethality in mice lacking protein phosphatase 2A catalytic subunit Calpha. *Proc Natl Acad Sci USA* 95:12370–12375.
27. Ruediger R, Ruiz J, Walter G (2011) Human cancer-associated mutations in the Aα subunit of protein phosphatase 2A increase lung cancer incidence in Aα knock-in and knockout mice. *Mol Cell Biol* 31:3832–3844.
28. Lee RH, Brown BM, Lolley RN (1984) Light-induced dephosphorylation of a 33K protein in rod outer segments of rat retina. *Biochemistry* 23:1972–1977.
29. Liu WB, et al. (2008) Differential expression of the catalytic subunits for PP-1 and PP-2A and the regulatory subunits for PP-2A in mouse eye. *Mol Vis* 14:762–773.
30. Li S, et al. (2005) Rhodopsin-iCre transgenic mouse line for Cre-mediated rod-specific gene targeting. *Genesis* 41:73–80.
31. Wang F, et al. (2012) RNAscope: A novel in situ RNA analysis platform for formalin-fixed, paraffin-embedded tissues. *J Mol Diagn* 14:22–29.
32. Gibson SK, Parkes JH, Liebman PA (2000) Phosphorylation modulates the affinity of light-activated rhodopsin for G protein and arrestin. *Biochemistry* 39:5738–5749.
33. Burns ME, Pugh EN, Jr (2009) RGS9 concentration matters in rod phototransduction. *Biophys J* 97:1538–1547.
34. Krispel CM, et al. (2006) RGS expression rate-limits recovery of rod photoresponses. *Neuron* 51:409–416.
35. Sundermeier TR, et al. (2014) R9AP overexpression alters phototransduction kinetics in iCre75 mice. *Invest Ophthalmol Vis Sci* 55:1339–1347.
36. Keller C, Grimm C, Wenzel A, Hafezi F, Remé C (2001) Protective effect of halothane anesthesia on retinal light damage: Inhibition of metabolic rhodopsin regeneration. *Invest Ophthalmol Vis Sci* 42:476–480.
37. Ohguro H, Palczewski K (1995) Separation of phospho- and non-phosphopeptides using reverse phase column chromatography. *FEBS Lett* 368:452–454.
38. Lee BY, Thulin CD, Willardson BM (2004) Site-specific phosphorylation of phosducin in intact retina. Dynamics of phosphorylation and effects on G protein beta gamma dimer binding. *J Biol Chem* 279:54008–54017.
39. Song H, Belcastro M, Young EJ, Sokolov M (2007) Compartment-specific phosphorylation of phosducin in rods underlies adaptation to various levels of illumination. *J Biol Chem* 282:23613–23621.
40. Kennedy MJ, Dunn FA, Hurley JB (2004) Visual pigment phosphorylation but not transducin translocation can contribute to light adaptation in zebrafish cones. *Neuron* 41:915–928.
41. Le YZ, et al. (2004) Targeted expression of Cre recombinase to cone photoreceptors in transgenic mice. *Mol Vis* 10:1011–1018.
42. Calvert PD, et al. (2000) Phototransduction in transgenic mice after targeted deletion of the rod transducin alpha-subunit. *Proc Natl Acad Sci USA* 97:13913–13918.
43. Carter-Dawson LD, LaVail MM (1979) Rods and cones in the mouse retina. I. Structural analysis using light and electron microscopy. *J Comp Neurol* 188:245–262.
44. Tobin AB (2008) G-protein-coupled receptor phosphorylation: Where, when and by whom. *Br J Pharmacol* 153:S167–S176.
45. Magalhaes AC, Dunn H, Ferguson SS (2012) Regulation of GPCR activity, trafficking and localization by GPCR-interacting proteins. *Br J Pharmacol* 165:1717–1736.
46. Pitcher JA, Payne ES, Csortos C, DePaoli-Roach AA, Lefkowitz RJ (1995) The G-protein-coupled receptor phosphatase: A protein phosphatase type 2A with a distinct subcellular distribution and substrate specificity. *Proc Natl Acad Sci USA* 92:8343–8347.
47. Kühn H (1974) Light-dependent phosphorylation of rhodopsin in living frogs. *Nature* 250:588–590.
48. Makino CL, et al. (2004) Recoverin regulates light-dependent phosphodiesterase activity in retinal rods. *J Gen Physiol* 123:729–741.
49. Sakurai K, Chen J, Khani SC, Kefalov VJ (2015) Regulation of mammalian cone phototransduction by recoverin and rhodopsin kinase. *J Biol Chem* 290:9239–9250.
50. Chen J, Makino CL, Peachey NS, Baylor DA, Simon MI (1995) Mechanisms of rhodopsin inactivation in vivo as revealed by a COOH-terminal truncation mutant. *Science* 267: 374–377.
51. Mendez A, et al. (2000) Rapid and reproducible deactivation of rhodopsin requires multiple phosphorylation sites. *Neuron* 28:153–164.
52. Doan T, Mendez A, Detwiler PB, Chen J, Rieke F (2006) Multiple phosphorylation sites confer reproducibility of the rod's single-photon responses. *Science* 313:530–533.
53. Azevedo AW, et al. (2015) C-terminal threonines and serines play distinct roles in the desensitization of rhodopsin, a G protein-coupled receptor. *Elife* 4:e05981.
54. Berry J, et al. (2016) Effect of rhodopsin phosphorylation on dark adaptation in mouse rods. *J Neurosci* 36:6973–6987.
55. Imai H, et al. (1997) Photochemical and biochemical properties of chicken blue-sensitive cone visual pigment. *Biochemistry* 36:12773–12779.
56. Ala-Laurila P, et al. (2006) Visual cycle: Dependence of retinol production and removal on photoproduct decay and cell morphology. *J Gen Physiol* 128:153–169.
57. Yamaoka H, Tachibanaki S, Kawamura S (2015) Dephosphorylation during bleach and regeneration of visual pigment in carp rod and cone membranes. *J Biol Chem* 290: 24381–24390.
58. Mustafi D, Maeda T, Kohno H, Nadeau JH, Palczewski K (2012) Inflammatory priming predisposes mice to age-related retinal degeneration. *J Clin Invest* 122:2989–3001.
59. Kiser PD, Golczak M, Palczewski K (2014) Chemistry of the retinoid (visual) cycle. *Chem Rev* 114:194–232.
60. Tang PH, Kono M, Koutalos Y, Ablonczy Z, Crouch RK (2013) New insights into retinoid metabolism and cycling within the retina. *Prog Retin Eye Res* 32:48–63.
61. Wang JS, Kefalov VJ (2011) The cone-specific visual cycle. *Prog Retin Eye Res* 30: 115–128.
62. Ohguro H, Van Hooser JP, Milam AH, Palczewski K (1995) Rhodopsin phosphorylation and dephosphorylation in vivo. *J Biol Chem* 270:14259–14262.
63. Kennedy MJ, et al. (2001) Multiple phosphorylation of rhodopsin and the in vivo chemistry underlying rod photoreceptor dark adaptation. *Neuron* 31:87–101.
64. Saari JC, et al. (2001) Visual cycle impairment in cellular retinaldehyde binding protein (CRALBP) knockout mice results in delayed dark adaptation. *Neuron* 29:739–748.
65. Weller M, Virmaux N, Mandel P (1975) Light-stimulated phosphorylation of rhodopsin in the retina: The presence of a protein kinase that is specific for photobleached rhodopsin. *Proc Natl Acad Sci USA* 72:381–385.
66. Azarian SM, King AJ, Hallett MA, Williams DS (1995) Selective proteolysis of arrestin by calpain. Molecular characteristics and its effect on rhodopsin dephosphorylation. *J Biol Chem* 270:24375–24384.
67. Palczewski K, McDowell JH, Jakes S, Ingebritsen TS, Hargrave PA (1989) Regulation of rhodopsin dephosphorylation by arrestin. *J Biol Chem* 264:15770–15773.
68. Lee KA, Nawrot M, Garwin GG, Saari JC, Hurley JB (2010) Relationships among visual cycle retinoids, rhodopsin phosphorylation, and phototransduction in mouse eyes during light and dark adaptation. *Biochemistry* 49:2454–2463.
69. Chen C, Blakeley LR, Koutalos Y (2009) Formation of all-*trans* retinol after visual pigment bleaching in mouse photoreceptors. *Invest Ophthalmol Vis Sci* 50:3589–3595.
70. Frederiksen R, et al. (2016) Rhodopsin kinase and arrestin binding control the decay of photoactivated rhodopsin and dark adaptation of mouse rods. *J Gen Physiol* 148: 1–11.
71. Grimm C, et al. (2004) Constitutive overexpression of human erythropoietin protects the mouse retina against induced but not inherited retinal degeneration. *J Neurosci* 24:5651–5658.
72. Mattapallil MJ, et al. (2012) The Rd8 mutation of the Crb1 gene is present in vendor lines of C57BL/6N mice and embryonic stem cells, and confounds ocular induced mutant phenotypes. *Invest Ophthalmol Vis Sci* 53:2921–2927.
73. Mears AJ, et al. (2001) Nrl is required for rod photoreceptor development. *Nat Genet* 29:447–452.
74. Golczak M, Bereta G, Maeda A, Palczewski K (2010) Molecular biology and analytical chemistry methods used to probe the retinoid cycle. *Methods Mol Biol* 652:229–245.
75. Vinberg F, Kolesnikov AV, Kefalov VJ (2014) Ex vivo ERG analysis of photoreceptors using an in vivo ERG system. *Vision Res* 101:108–117.
76. Sillman AJ, Ito H, Tomita T (1969) Studies on the mass receptor potential of the isolated frog retina. I. General properties of the response. *Vision Res* 9:1435–1442.
77. Nymark S, Heikkinen H, Haldin C, Donner K, Koskelainen A (2005) Light responses and light adaptation in rat retinal rods at different temperatures. *J Physiol* 567:923–938.
78. Arino J, Woon CW, Brautigan DL, Miller TB, Jr, Johnson GL (1988) Human liver phosphatase 2A: cDNA and amino acid sequence of two catalytic subunit isotypes. *Proc Natl Acad Sci USA* 85:4252–4256.
79. Khew-Goodall Y, Mayer RE, Maurer F, Stone SR, Hemmings BA (1991) Structure and transcriptional regulation of protein phosphatase 2A catalytic subunit genes. *Biochemistry* 30:89–97.
80. Lee EC, et al. (2001) A highly efficient *Escherichia coli*-based chromosome engineering system adapted for recombinogenic targeting and subcloning of BAC DNA. *Genomics* 73:56–65.
81. Wu Y, Wang C, Sun H, LeRoith D, Yakar S (2009) High-efficient FLPo deleter mice in C57BL/6J background. *PLoS One* 4:e8054.
82. Pepperberg DR, et al. (1992) Light-dependent delay in the falling phase of the retinal rod photoresponse. *Vis Neurosci* 8:9–18.
83. Woodruff ML, Lem J, Fain GL (2004) Early receptor current of wild-type and transducin knockout mice: Photosensitivity and light-induced Ca^{2+} release. *J Physiol* 557: 821–828.
84. Nikonov SS, Kholodenko R, Lem J, Pugh EN, Jr (2006) Physiological features of the S- and M-cone photoreceptors of wild-type mice from single-cell recordings. *J Gen Physiol* 127:359–374.